BIOCHEMISTRY
including biophysical chemistry & molecular biology
Article

Biochemistry **2009,** *48,* 5769–5778 5769
DOI: 10.1021/bi900636c

Hydron Transfer Catalyzed by Triosephosphate Isomerase. Products of the Direct and Phosphite-Activated Isomerization of [1-^{13}C]-Glycolaldehyde in D_2O†

Maybelle K. Go, Tina L. Amyes, and John P. Richard*

Department of Chemistry, University at Buffalo, SUNY, Buffalo, New York 14260-3000

Received April 13, 2009

ABSTRACT: Product distributions for the reaction of glycolaldehyde labeled with carbon-13 at the carbonyl carbon ([1-^{13}C]-GA) catalyzed by triosephosphate isomerase (TIM) in D_2O at pD 7.0 in the presence of phosphite dianion and in its absence were determined by ^{1}H NMR spectroscopy. We observe three products for the relatively fast phosphite-activated reaction (Amyes, T. L., and Richard, J. P. (2007) *Biochemistry 46*, 5841−5854): [2-^{13}C]-GA from isomerization with intramolecular transfer of hydrogen (12% of products), [2-^{13}C,2-^{2}H]-GA from isomerization with incorporation of deuterium from D_2O at C-2 (64% of products), and [1-^{13}C,2-^{2}H]-GA from incorporation of deuterium from D_2O at C-2 (23% of products). The much slower unactivated reaction in the absence of phosphite results in formation of the same three products along with the doubly deuterated product [1-^{13}C,2,2-$^2H_2$]-GA. The two isomerization products ([2-^{13}C]-GA and [2-^{13}C,2-^{2}H]-GA) are formed in the same relative yields in both the unactivated and the phosphite-activated reactions. However, the additional [1-^{13}C,2-^{2}H]-GA and the doubly deuterated [1-^{13}C,2,2-$^2H_2$]-GA formed in the unactivated TIM-catalyzed reaction are proposed to result from *nonspecific* reaction(s) at the protein surface. The data provide evidence that phosphite dianion affects the rate, but not the product distribution, of the TIM-catalyzed reaction of [1-^{13}C]-GA at the enzyme active site. They are consistent with the conclusion that both reactions occur at an unstable loop-closed form of TIM and that activation of the isomerization reaction by phosphite dianion results from utilization of the intrinsic binding energy of phosphite dianion to stabilize the active loop-closed enzyme.

Triosephosphate isomerase (TIM)[1] catalyzes the stereospecific, reversible 1,2-hydrogen shift at dihydroxyacetone phosphate (DHAP) to give (*R*)-glyceraldehyde 3-phosphate (GAP) by a single-base (Glu-165) proton transfer mechanism through an enzyme-bound *cis*-enediol(ate) intermediate (Scheme 1) (*1*, *2*). The enzyme's low molecular mass (dimer, 26 kDa/subunit), high cellular abundance (*3*), and the centrality of proton transfer at carbon in metabolic processes (*4*, *5*) have made TIM a prominent target for studies on the mechanism of enzyme action (*6*−*8*).

Scheme 1

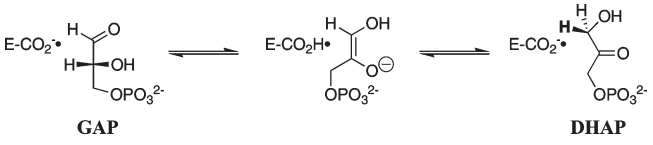

GAP **DHAP**

We showed previously that deprotonation of the neutral substrate (*R*)-glyceraldehyde by TIM is ca. 10^9-fold slower than the partly diffusion controlled (*9*) turnover of the physiological phosphorylated substrate GAP (*10*). More than 80% of the 4×10^{10}-fold enzymatic rate acceleration for deprotonation of GAP is due to utilization of the intrinsic binding energy of the small nonreacting phosphodianion group of the substrate (*10*, *11*). Part of this "intrinsic phosphate binding energy" is expressed at the Michaelis complex and serves the obvious function of anchoring the substrate to TIM. However, these results suggested that a large fraction of this binding energy is utilized to activate the bound carbon acid substrate toward proton transfer.

Our work is now focused on understanding the role of flexible "phosphate gripper loops", such as loop 6 of TIM (*6*, *12*−*18*), in activating enzyme-bound substrates for a variety of reactions (*19*, *20*). We reported earlier that TIM catalyzes the slow deprotonation of glycolaldehyde (GA) in D_2O, resulting in deuterium labeling of GA at C-2 that can be monitored by ^{1}H NMR spectroscopy (Scheme 2), with a second-order rate constant $k_{cat}/K_m = 0.26\ M^{-1}\ s^{-1}$ (*19*). The addition of exogenous phosphite dianion results in a very large increase in the observed second-order rate constant $(k_{cat}/K_m)_{obsd}$ for turnover of GA, and the plot of $(k_{cat}/K_m)_{obsd}$ against $[HPO_3^{2-}]$ provides evidence for saturation of the enzyme by phosphite. The data show

†This work was supported by Grant GM39754 from the National Institutes of Health.

*Author to whom correspondence should be addressed. Tel: (716) 645 4232. Fax: (716) 645 6963. E-mail: jrichard@buffalo.edu.

[1]Abbreviations: TIM, triosephosphate isomerase; DHAP, dihydroxyacetone phosphate; GAP, (*R*)-glyceraldehyde 3-phosphate; GA, glycolaldehyde; GPDH, glycerol 3-phosphate dehydrogenase; BSA, bovine serum albumin; NADH, nicotinamide adenine dinucleotide, reduced form; NMR, nuclear magnetic resonance.

Published on Web 05/08/2009

Scheme 2

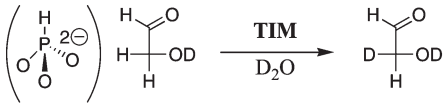

GA **[2-^{2}H]-GA**

that the *separate* binding of the phosphite dianion "piece" to TIM results in a 700-fold acceleration of proton transfer from carbon (Scheme 2) (*19*). This demonstration that the interactions between TIM and phosphite dianion activate a bound carbon acid substrate toward deprotonation, in the absence of a covalent connection, shows that the phosphodianion group of GAP does not simply anchor the substrate to the enzyme. Rather, it also serves the additional important function of providing binding energy that is utilized specifically for transition state stabilization (*19*, *21*). We proposed that the phosphite activation of TIM can be attributed to utilization of the intrinsic phosphite binding energy to hold TIM in a catalytically active loop-closed form (*19*).

The TIM-catalyzed reactions of the whole substrates GAP and DHAP in D_2O give complex mixtures of products, as shown in Scheme 3 for the reaction of GAP (*22*, *23*). This mixture results from partitioning of the enediol(ate) phosphate intermediate at two different stages of the overall reaction (*1*, *24*). Proton transfer from GAP to the carboxylate side chain of Glu-165 labels the side chain with H. In D_2O, this labeled side chain partitions between reprotonation of the enediol(ate) phosphate at C-1 to form H-labeled DHAP (49% yield) and effectively irreversible exchange with deuterium from solvent D_2O (k_{ex}, Scheme 3). The D-labeled side chain then partitions between reaction of the enediol(ate) phosphate at C-2 to form D-labeled GAP (21% yield) and at C-1 to form D-labeled DHAP (31% yield) (*22*).

Scheme 3

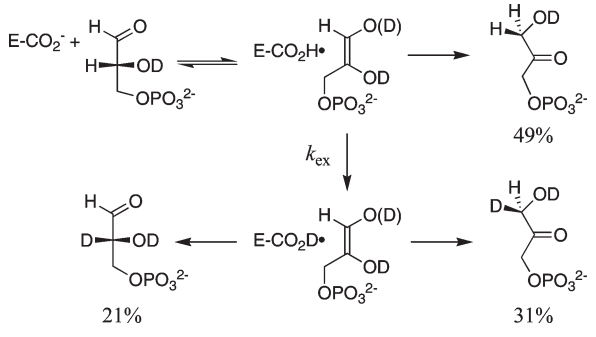

It is not known whether TIM catalyzes hydrogen transfer between the hydroxymethylene and carbonyl carbons of glycolaldehyde (GA) because this formal isomerization reaction is degenerate. Therefore, reaction of the D-labeled side chain of Glu-165 with the putative enediol(ate) intermediate of the TIM-catalyzed deprotonation of GA results in formation of only one product, [2-^{2}H]-GA (*19*). We have therefore extended our comparison of TIM-catalyzed isomerization of the whole substrates GAP and DHAP with that of the substrate pieces {GA + HPO_3^{2-}} to an examination of the product distribution for the TIM-catalyzed reaction of [1-^{13}C]-glycolaldehyde ([1-^{13}C]-GA) in D_2O, in both the presence and absence of phosphite dianion.

We report here that the phosphite-activated TIM-catalyzed reaction of [1-^{13}C]-GA in D_2O gives the three expected products

Chart 1

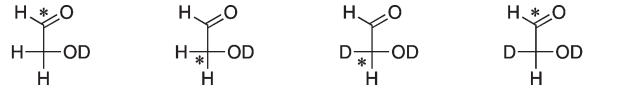

[1-^{13}C]-GA **[2-^{13}C]-GA** **[2-^{13}C, 2-^{2}H]-GA** **[1-^{13}C, 2-^{2}H]-GA**

of partitioning of the enzyme-bound enediol(ate) intermediate (see Chart 1), in yields similar to those of the corresponding products of the TIM-catalyzed reactions of the whole substrates GAP (*22*) and DHAP (*23*). Moreover, similar yields of these products are observed for the unactivated TIM-catalyzed reaction of [1-^{13}C]-GA in D_2O in the absence of phosphite. These results suggest that the active catalyst for the slow isomerization of [1-^{13}C]-GA is an unstable loop-closed form of TIM and that the intrinsic binding energy of phosphite dianion is utilized to stabilize the enzyme in the active loop-closed form.

MATERIALS AND METHODS

Rabbit muscle glycerol 3-phosphate dehydrogenase (GPDH) was purchased from United States Biochemical or MP Biomedicals. Bovine serum albumin (BSA) was from Roche. DEAE-Sepharose Fast Flow was from GE Healthcare. D,L-Glyceraldehyde 3-phosphate diethyl acetal (barium salt), dihydroxyacetone phosphate (lithium salt), Dowex 50WX4-200R and NADH (disodium salt) were from Sigma. Triethanolamine hydrochloride and imidazole were from Aldrich. Sodium phosphite (dibasic, pentahydrate) was from Riedel-de Haen (Fluka). [1-^{13}C]-Glycolaldehyde (99% enriched with ^{13}C at C-1, 0.09 M in water) was purchased from Omicron Biochemicals. D_2O (99.9% D) and DCl (35% w/w, 99.9% D) were from Cambridge Isotope Laboratories. Imidazole was recrystallized from benzene. Water was from a Milli-Q Academic purification system. All other commercially available chemicals were reagent grade or better and were used without further purification.

The plasmid pBSX1cTIM containing the wild-type gene for TIM from chicken muscle (*25*) and *Escherichia coli* strain DF502 (strep^R, tpi$^-$, and his$^-$) whose DNA lacks the gene for TIM (*26*) were generous gifts from Professor Nicole Sampson. *E. coli* strain DF502 was transformed with pBSX1cTIM, and TIM was expressed and purified according to published procedures with ion-exchange chromatography performed on DEAE-Sepharose (*15*). The enzyme obtained from the final column was judged to be homogeneous by gel electrophoresis. The concentration of TIM was determined from the absorbance at 280 nm using an extinction coefficient of 3.2×10^4 M^{-1} cm^{-1} (*27*). The following kinetic parameters were determined for turnover of GAP in 30 mM triethanolamine buffer at pH 7.5 and 25 °C (I = 0.1, NaCl) using a coupled assay (see below): k_{cat} = 2300 s^{-1} and K_m = 0.45 mM (*22*).

Preparation of Solutions. Solution pH or pD was determined at 25 °C using an Orion model 720A pH meter equipped with a Radiometer pHC4006-9 combination electrode that was standardized at pH 4.00 and 7.00 at 25 °C. Values of pD were obtained by adding 0.40 to the observed reading of the pH meter (*28*). Before preparation of solutions in D_2O the bulk of the water of crystallization of sodium phosphite was removed by drying *in vacuo* as described previously (*19*). Buffered solutions of 30 mM imidazole (20% free base, pD 7.0) and 80 mM phosphite (50% free base, pD 7.0) in D_2O were prepared as described previously (*19*).

D,L-Glyceraldehyde 3-phosphate diethyl acetal (barium salt) was converted to the free aldehyde by treatment with a suspension of Dowex 50WX4-200R (H^+ form) in boiling water, as described previously (*22*), and the resulting solution of D,L-glyceraldehyde 3-phosphate (pH ≈ 2) was stored at −20 °C. Before use in routine enzyme assays the solution was adjusted to the appropriate pH by the addition of 1 M NaOH, after which it was stored at −20 °C. The concentration of GAP in the racemic mixture was determined from the amount of NADH consumed during quantitative TIM-catalyzed isomerization of GAP to form DHAP that was coupled to the oxidation of NADH using GPDH.

[1-^{13}C]-Glycolaldehyde (1 mL of a 90 mM solution in H_2O) was reduced to a volume of ca. 100 μL by rotary evaporation. Five milliliters of D_2O was added, and the volume was again reduced to ca. 100 μL by rotary evaporation. This procedure was repeated twice more, and ca. 900 μL of D_2O was added to the final solution to give a final volume of ca. 1 mL. The stock solution of [1-^{13}C]-GA in D_2O was stored at room temperature to minimize the content of glycolaldehyde dimer (*19*), and the concentration of [1-^{13}C]-GA was determined by ^{1}H NMR spectroscopy as follows. Fifty microliters of the stock solution of [1-^{13}C]-GA in D_2O was diluted with 700 μL of 30 mM imidazole buffer (20% free base, pD 7.0) in D_2O, and the concentration of [1-^{13}C]-GA was determined from comparison of the integrated areas of the signals for the protons of [1-^{13}C]-GA hydrate and the C(4,5)-protons of imidazole, with a correction for the presence of 6.1% of the free carbonyl form of GA that is present in equilibrium with the hydrate (*19*, *29*).

Enzyme Assays. All enzyme assays were carried out at 25 °C. Changes in the concentration of NADH were calculated from the changes in absorbance at 340 nm using an extinction coefficient of 6220 M^{-1} cm^{-1}. One unit is the amount of enzyme that converts 1 μmol of substrate to product in 1 min under the specified conditions.

GPDH was dialyzed against 20 mM triethanolamine buffer (pH 7.5) at 4 °C and was assayed by monitoring the oxidation of NADH by DHAP at 340 nm. The assay mixture contained 100 mM triethanolamine (pH 7.5, I = 0.1), 0.01% BSA, 0.2 mM NADH, and 1 mM DHAP.

The activity of TIM in the stock solutions dialyzed in D_2O or of the diluted reaction mixtures in D_2O was assayed by coupling the isomerization of GAP to give DHAP to the oxidation of NADH by DHAP using GPDH, monitored at 340 nm as described previously (*19*, *30*). Dilute solutions of TIM were stabilized with 0.01% BSA. The standard assay mixture (1.0 mL) contained 100 mM triethanolamine (pH 7.5, I = 0.1), 0.2 mM NADH, 5 mM D,L-glyceraldehyde 3-phosphate (2.5 mM GAP, ≈ 6 K_m), 1 unit of GPDH, and 0.01−0.05 nM TIM. Before the addition of TIM, the low background velocity that is due mainly to the isomerization of GAP catalyzed by TIM present as a contaminant in the commercial GPDH was determined over 2−4 min. This background velocity, v_o, generally represented ≤2% of the total initial velocity, v_i, that was determined subsequently over 5−10 min after the addition of TIM. Values of V_{max} ($M\ s^{-1}$) were calculated from the values of ($v_i - v_o$) using the initial concentration of GAP and K_m = 0.45 mM. The concentration of TIM in the assay mixture was calculated from the values of V_{max} ($M\ s^{-1}$) using the relationship [TIM] = V_{max}/k_{cat} with k_{cat} = 2300 s^{-1}.

TIM-Catalyzed Reactions of [1-^{13}C]-GA Monitored by ^{1}H NMR. Chicken muscle TIM was dialyzed at 4 °C against 30 mM imidazole buffer (20% free base, pD 7.0) in D_2O at I = 0.024 for reactions in the presence of phosphite dianion or at I = 0.1 (NaCl) for reactions in its absence.

The TIM-catalyzed reactions of [1-^{13}C]-GA in D_2O in the absence of phosphite were initiated by adding 720 μL of TIM (ca. 85 units/μL, 16 mg/mL) in 30 mM imidazole buffer (20% free base, pD 7.0) at I = 0.1 (NaCl) in D_2O to 180 μL of a solution of [1-^{13}C]-GA and NaCl in D_2O to give final concentrations of 20 mM [1-^{13}C]-GA and 24 mM imidazole at pD 7.0 and I = 0.1 (NaCl). This solution (750 μL) was transferred to an NMR tube, and ^{1}H NMR spectra at 25 °C (32 transients) were recorded hourly over a period of ca. 24 h, during which time there was ca. 29% reaction of [1-^{13}C]-GA. The remaining portion of the reaction mixture was incubated at 25 °C, and the activity of TIM was determined via periodic standard assay (see above).

The TIM-catalyzed reactions of [1-^{13}C]-GA in D_2O in the presence of phosphite dianion were initiated by adding 5−20 μL of TIM (ca. 64 units/μL, 12 mg/mL) in 30 mM imidazole buffer (20% free base, pD 7.0) at I = 0.024 in D_2O to 1.0 mL of a solution containing 20 mM [1-^{13}C]-GA, 6 mM imidazole (20% free base, pD 7.0), and 5−20 mM phosphite dianion at pD 7.0 and I = 0.1 (NaCl). The final reaction mixture contained 20 mM [1-^{13}C]-GA, 6 mM imidazole, and 5−20 mM phosphite dianion (10−40 mM total phosphite) at pD 7.0 and I = 0.1 (NaCl). This solution (750 μL) was transferred to an NMR tube, and ^{1}H NMR spectra at 25 °C (32 transients) were recorded hourly over a period of ca. 12 h, during which time there was ca. 23% reaction of [1-^{13}C]-GA. The remaining portion of the reaction mixture was incubated at 25 °C, and the activity of TIM was determined via periodic standard assay (see above).

For the reactions in both the absence and presence of phosphite dianion there was no significant decrease in enzyme activity (±10%) during the course of the experiment. After accumulation of the final NMR spectrum the protein was removed by ultrafiltration, and the pD of the filtrate was determined and found to be within 0.05 unit of the initial value of 7.0.

^{1}H NMR Analyses. ^{1}H NMR spectra (500 MHz) were recorded in D_2O at 25 °C using a Varian Unity Inova 500 spectrometer that was shimmed to give a line width of ≤0.5 Hz for the most downfield peak of the double triplet due to the C-1 proton of [1-^{13}C]-GA hydrate. Spectra (32 transients) were obtained using a sweep width of 6000 Hz, a pulse angle of 90°, and an acquisition time of 6 s. To ensure accurate integrals for the protons of interest, a relaxation delay of 120 s ($> 8T_1$) was used (*19*). Baselines were subjected to a first-order drift correction before determination of integrated peak areas. Chemical shifts are reported relative to HOD at 4.67 ppm.

Determination of Product Yields by ^{1}H NMR. Figure 1 shows representative partial ^{1}H NMR spectra at 500 MHz obtained during the reaction of [1-^{13}C]-GA (20 mM) catalyzed by chicken muscle TIM in D_2O in the presence of 5 mM phosphite dianion (panels A and B) and in its absence (panels C and D) at pD 7.0 and 25 °C (I = 0.1, NaCl). These reactions resulted in formation of the isotopomers of GA hydrate shown in Chart 2. Under our reaction conditions glycolaldehyde exists as 94% of the hydrate and only 6% of the free carbonyl form (*19*, *29*). The integrated peak areas for the C-1 proton and for a *single* C-2 proton of the *hydrates* of the substrate [1-^{13}C]-GA and of each of the product isotopomers were obtained using the following procedures.

[1-^{13}C]-GA (Substrate). The signal for the C-1 proton of [1-^{13}C]-GA appears as a double triplet at 4.945 ppm ($^{1}J_{HC}$ = 163 Hz, $^{3}J_{HH}$ = 5 Hz) (tall signals at edges of Figure 1A). The peak area for this proton was evaluated using eq 1, where *a* is the area of the most downfield peak of the double triplet. The signal for the C-2 protons of [1-^{13}C]-GA appears as a double doublet at 3.410 ppm ($^{2}J_{HC}$ = 3 Hz, $^{3}J_{HH}$ = 5 Hz) (offscale signal in the center of Figure 1B). The partly resolved small multiplet on the upfield edge of this signal (Figure 1B, inset) is the signal for the C-2 proton of [1-^{13}C,2-^{2}H]-GA, the product of deuterium exchange (see below). The peak area for a *single* C-2 proton of [1-^{13}C]-GA was evaluated using eq 2, where A_T is the total area of the signals for the C-2 protons of *both* [1-^{13}C]-GA and [1-^{13}C,2-^{2}H]-GA, and 2*e* is the area of the small multiplet due to the C-2 proton of [1-^{13}C,2-^{2}H]-GA (obtained as described below).

$$A_{C1} = 8a \quad (1)$$

$$A_{C2} = (A_T - 2e)/2 \quad (2)$$

[2-^{13}C]-GA (Product of Isomerization). The signal for the C-1 proton of [2-^{13}C]-GA appears as a broad triplet at 4.945 ppm ($^{2}J_{HC}$ = 0.5 Hz, $^{3}J_{HH}$ = 5 Hz; the HC coupling was not always observed). However, only the most downfield peak of this signal is observable (Figure 1A, inset) because the upfield peaks are obscured by the broad doublet due to the C-1 proton of [2-^{13}C,2-^{2}H]-GA, the product of isomerization with deuterium exchange (see below). The peak area for the C-1 proton of [2-^{13}C]-GA was evaluated using eq 3, where *b* is the area of the most downfield peak of the broad triplet. The signal for the C-2 protons of [2-^{13}C]-GA appears as a double doublet at 3.410 ppm ($^{1}J_{HC}$ = 142 Hz, $^{3}J_{HH}$ = 5 Hz) (small signals at the edges of Figure 1B). The very small signals at the base of the peaks of this signal (Figure 1B, inset) are the ^{13}C satellites of the very large double doublet for [1-^{13}C]-GA arising from the presence of natural abundance ^{13}C at C-2 of [1-^{13}C]-GA. The peak area for a *single* C-2 proton of [2-^{13}C]-GA was evaluated using eq 4, where *c* is the area of the most downfield peak of the double doublet (Figure 1B, inset). The values of A_{C1} and A_{C2} were corrected for the presence of a small amount (ca. 0.8%) of [2-^{13}C]-GA that was present at zero time as an impurity in the commercial sample of [1-^{13}C]-GA.

$$A_{C1} = 4b \quad (3)$$

$$A_{C2} = 2c \quad (4)$$

[1-^{13}C,2-^{2}H]-GA (Product of Deuterium Exchange). The signal for the C-1 proton of [1-^{13}C,2-^{2}H]-GA appears as a broad double doublet at 4.940 ppm shifted 0.005 ppm upfield of the double triplet due to the C-1 proton of [1-^{13}C]-GA as a result of the β-deuterium (*19*). However, this signal is not resolved; it lies under the two most upfield peaks of each half of the double triplet due to the C-1 proton of [1-^{13}C]-GA. Thus, for all intents and purposes, we will refer to the signal for the C-1 proton of [1-^{13}C]-GA as an *apparent* double triplet (Figure 1A). The peak area for the C-1 proton of [1-^{13}C,2-^{2}H]-GA was evaluated using eq 5, where A_T is the area of downfield half of the *apparent* double

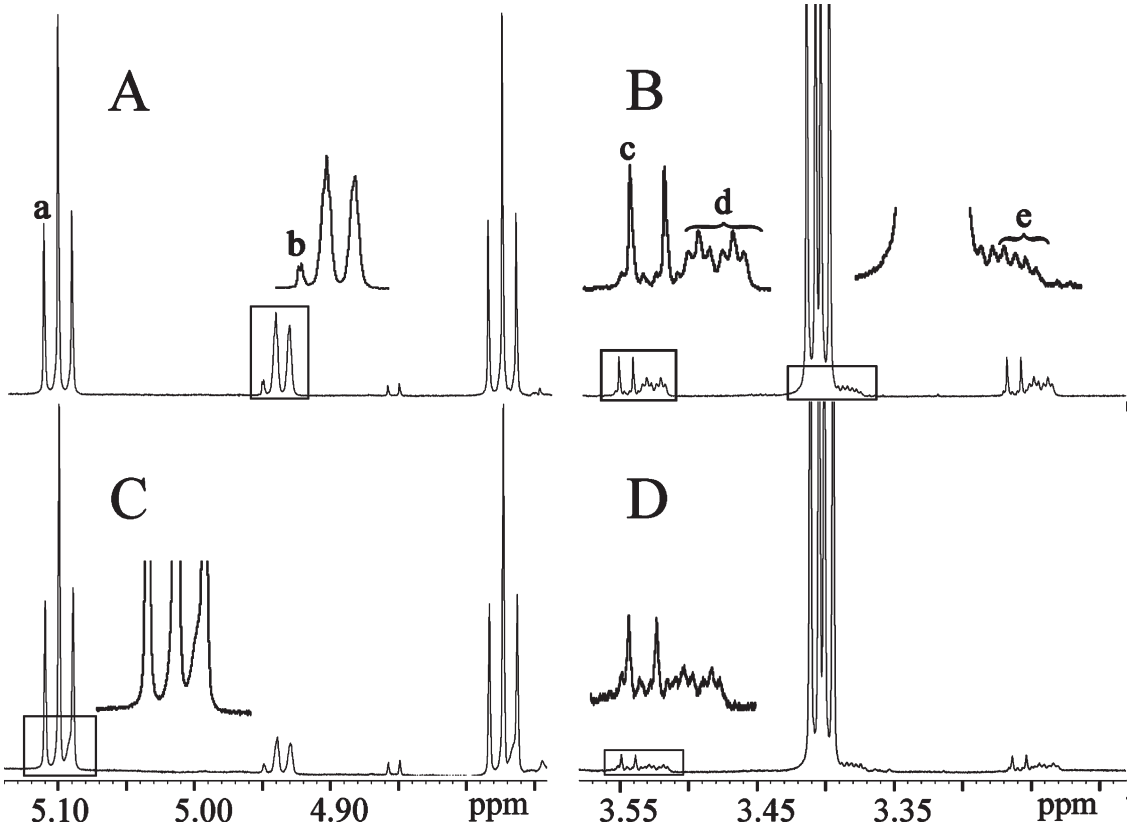

FIGURE 1: Partial ^{1}H NMR spectra at 500 MHz in the C-1 and C-2 regions of glycolaldehyde hydrate obtained during the reaction of [1-^{13}C]-GA catalyzed by chicken muscle TIM in D_2O at pD 7.0 and 25 °C (I = 0.1, NaCl). The boxes indicate regions of the spectrum that are expanded in the insets. (A) Spectrum in the region of the C-1 proton obtained after reaction of 23% of [1-^{13}C]-GA (20 mM) in the presence of 7.9 μM TIM and 5 mM HPO_3^{2-}. (B) Spectrum in the C-2 region for the phosphite-activated reaction. (C) Spectrum in the C-1 region obtained after reaction of 29% of [1-^{13}C]-GA (20 mM) catalyzed by 340 μM TIM in the absence of phosphite dianion. (D) Spectrum in the C-2 region for the reaction in the absence of phosphite.

Chart 2

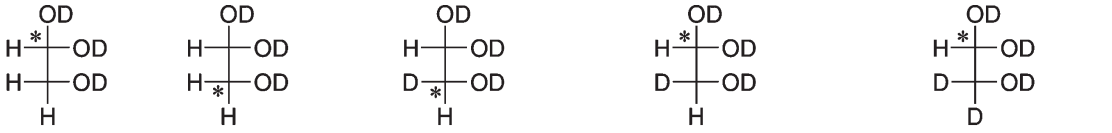

[1-^{13}C]-GA [2-^{13}C]-GA [2-^{13}C, 2-^{2}H]-GA [1-^{13}C, 2-^{2}H]-GA [1-^{13}C, 2,2-di-^{2}H]-GA

triplet due to the C-1 proton of [1-^{13}C]-GA, and *a* is the area of the most downfield peak of this *apparent* double triplet. This analysis is possible because *a* represents a signal that is due exclusively to the C-1 proton of [1-^{13}C]-GA. The signal for the C-2 proton of [1-^{13}C,2-^{2}H]-GA appears as a multiplet on the upfield edge of the signal for the C-2 protons of [1-^{13}C]-GA and is expected to be a double double triplet as a result of a three-bond HH coupling (J = 5 Hz), a two-bond HC coupling (J = 3 Hz), and a two-bond HD coupling ($J \approx 2$ Hz). The observed multiplet is composed of eight peaks, and its peak area was evaluated from the integrated area *e* of the four most upfield peaks of this signal using eq 6 (Figure 1B, inset).

$$A_{C1} = 2A_T - 8a \quad (5)$$

$$A_{C2} = 2e \quad (6)$$

[2-^{13}C,2-^{2}H]-GA (Product of Isomerization with Deuterium Exchange). The signal for the C-1 proton of [2-^{13}C,2-^{2}H]-GA appears as a broad doublet at 4.940 ppm ($^{3}J_{HH}$ = 5 Hz, the three-bond HD and two-bond HC couplings are not resolved) (Figure 1A, inset). This doublet obscures the upfield peaks of the broad triplet due to the C-1 proton of [2-^{13}C]-GA (see above). The peak area for the C-1 proton of [2-^{13}C,2-^{2}H]-GA was evaluated using eq 7, where A_T is the total area of the signals for the C-1 protons of *both* [2-^{13}C,2-^{2}H]-GA and [2-^{13}C]-GA and *b* is the area of the most downfield peak of the broad triplet due to the C-1 proton of [2-^{13}C]-GA. The signal for the C-2 proton of [2-^{13}C,2-^{2}H]-GA appears as a double double triplet at 3.389 ppm ($^{1}J_{HC}$ = 142 Hz, $^{3}J_{HH}$ = 5 Hz, $^{2}J_{HD} \approx 2$ Hz) shifted 0.021 ppm upfield of the double doublet due to the C-2 protons of [2-^{13}C]-GA as a result of the α-deuterium (Figure 1B, inset) (*19*, *31*−*33*). The peak area for the C-2 proton of [2-^{13}C,2-^{2}H]-GA was evaluated using eq 8, where *d* is the area of the downfield half of the double double triplet (Figure 1B, inset).

$$A_{C1} = A_T - 4b \quad (7)$$

$$A_{C2} = 2d \quad (8)$$

The observed peak areas A_{obs} for these different protons at various reaction times were normalized according to eq 9 to give A_P, where A_{std} and $(A_{std})_0$ are the observed peak areas for an internal standard at time t and at t = 0, respectively. The internal standard was the upfield peak of the doublet at 6.7 ppm (J = 600 Hz) due to the P−H proton of phosphite or the signal at 7.3 ppm due to the C-(4,5) protons of imidazole.

The disappearance of the substrate [1-^{13}C]-GA was followed by monitoring the decrease in the peak area for the C-1 proton of [1-^{13}C]-GA that was calculated using eq 1. The fraction of the substrate [1-^{13}C]-GA remaining at time t, f_S, was calculated using eq 10, where A_S and $(A_S)_0$ are the normalized peak areas for the C-1 proton of [1-^{13}C]-GA at time t and t = 0, respectively (cf. eq 9). Observed first-order rate constants k_{obsd} (s^{-1}) for the disappearance of [1-^{13}C]-GA were determined from the slopes of

Scheme 4

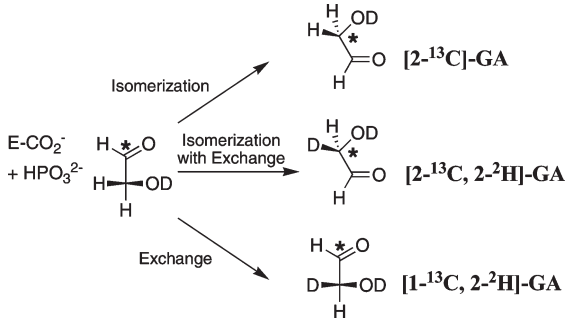

semilogarithmic plots of reaction progress against time (eq 11) that covered the first 30% of the reaction.

The *normalized* yields of the individual products of the TIM-catalyzed reactions of [1-^{13}C]-GA (Chart 2) were calculated using eq 12, where A_P is the normalized peak area for a single C-1 or C-2 proton of the individual product calculated using eq 9, and $\sum A_P$ is the sum of the normalized peak areas for the same proton at all of the reaction products.

$$A_P = A_{obs}\left(\frac{(A_{std})_0}{A_{std}}\right) \quad (9)$$

$$f_S = \frac{A_S}{(A_S)_0} \quad (10)$$

$$\ln f_S = -k_{obsd}t \quad (11)$$

$$f_P = \frac{A_P}{\sum A_P} \quad (12)$$

RESULTS

TIM-Catalyzed Reactions of [1-^{13}C]-GA Activated by Phosphite Dianion. Panels A and B of Figure 1 show partial ^{1}H NMR spectra at 500 MHz in the region of the C-1 and C-2 protons, respectively, obtained after the reaction of 23% of [1-^{13}C]-GA (20 mM) catalyzed by chicken muscle TIM (7.9 μM) in D_2O in the presence of 5 mM phosphite dianion at pD 7.0, 25 °C, and I = 0.1 (NaCl). The disappearance of the signals due to the substrate [1-^{13}C]-GA is accompanied by the appearance of signals due to the three isotopomeric products of the isomerization and deuterium exchange reactions shown in Scheme 4. Full details of the assignments of the signals for the C-1 and C-2 protons of the substrate and these products are given in the Materials and Methods. Normalized peak areas for the C-1 proton and a *single* C-2 proton of the substrate and of the individual products were calculated using eq 9. There is good agreement between the *decrease* in the normalized peak area for a *single* C-2 proton of the substrate [1-^{13}C]-GA and the *increase* in the sum of the normalized peak areas for a *single* C-2 proton of the products [2-^{13}C]-GA, [2-^{13}C,2-^{2}H]-GA, and [1-^{13}C,2-^{2}H]-GA. This shows that these

are the only significant products of the TIM-catalyzed reaction of [1-^{13}C]-GA activated by phosphite dianion.

The TIM-catalyzed incorporation of deuterium into [1-^{13}C]-GA to give [1-^{13}C,2-^{2}H]-GA and [2-^{13}C,2-^{2}H]-GA results in a large upfield shift of 0.021 ppm of the signal for the remaining C-2 proton of these compounds as a result of the α-deuterium (*19*, *31*−*33*). Thus, the signals for the C-2 protons of these products are well-resolved from those due to the C-2 protons of the substrate [1-^{13}C]-GA and the isomerization product [2-^{13}C]-GA (Figure 1B, peaks d and e). By contrast, the signals for the C-1 protons of [1-^{13}C,2-^{2}H]-GA and [2-^{13}C,2-^{2}H]-GA are not resolved from those for [1-^{13}C]-GA and [2-^{13}C]-GA because there is only a small upfield shift of 0.005 ppm as a result of the β-deuterium (Figure 1A) (*19*). For example, the ratio of the areas of the three downfield peaks of the *apparent* double triplet due to the C-1 proton of [1-^{13}C]-GA in Figure 1A is 1.00:2.18:1.17, rather than the expected 1.00:2.00:1:00. This is because the two most upfield peaks lie over those of the double doublet due to the C-1 proton of the deuterium exchange product [1-^{13}C,2-^{2}H]-GA. The Materials and Methods section describes in detail the procedures that were used to calculate the relative yields of the three products of isomerization and deuterium exchange using either the poorly resolved signals for the C-1 protons or the better resolved signals for the C-2 protons. In all cases there was acceptable agreement between the yields of the reaction products determined using both approaches.

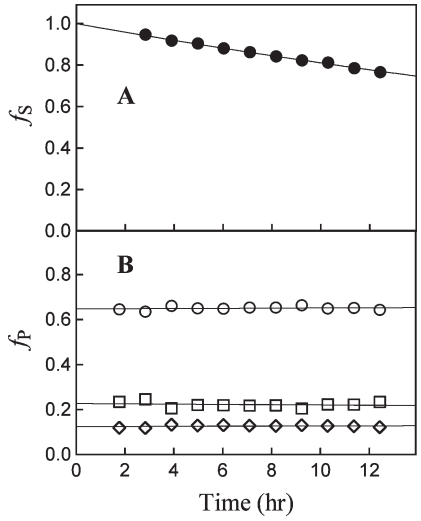

FIGURE 2: Dependence of the fraction of remaining substrate and the normalized fractions of the products during the reaction of [1-^{13}C]-GA (20 mM) catalyzed by chicken muscle TIM (7.9 μM) in the presence of 5 mM HPO_3^{2-} in D_2O at pD 7.0 and 25 °C (I = 0.1, NaCl). (A) The decrease with time in the fraction of remaining [1-^{13}C]-GA, calculated using eq 10. (B) The change with time in the fractional yields of the products of the phosphite-activated TIM-catalyzed reaction of [1-^{13}C]-GA calculated using eq 12. Extrapolations of these data to zero time gave the initial normalized product yields f_E that are reported in Table 1. Key: ◇, [2-^{13}C]-GA; □, [1-^{13}C,2-^{2}H]-GA; ○, [2-^{13}C,2-^{2}H]-GA.

The fraction of the [1-^{13}C]-GA substrate remaining, f_s, and the fractional yields of each of the products, f_P, were determined from the normalized peak areas for the protons of the reactants and products using eqs 10 and 12, respectively. Figure 2A shows the decrease with time in the fraction of remaining substrate, f_s, during the reaction of [1-^{13}C]-GA (20 mM) catalyzed by chicken muscle TIM (7.9 μM) in D_2O in the presence of 5 mM phosphite dianion at pD 7.0, 25 °C, and I = 0.1 (NaCl). Figure 2B shows the fractional yields of the products [2-^{13}C]-GA, [2-^{13}C,2-^{2}H]-GA, and [1-^{13}C,2-^{2}H]-GA, f_P, determined during the first ca. 20% of this reaction. The *initial normalized* product yields, f_E, obtained from short extrapolations of the observed yields to zero time, are reported in Table 1. The same procedure was used to determine the product yields for the TIM-catalyzed reactions of [1-^{13}C]-GA activated by 10 and 20 mM phosphite dianion (Table 1).

First-order rate constants, k_{obsd} (s^{-1}), for the TIM-catalyzed reactions of [1-^{13}C]-GA were determined by monitoring the disappearance of [1-^{13}C]-GA by ^{1}H NMR (eq 11). Table 1 reports the apparent second-order rate constants $(k_{cat}/K_m)_{obsd}$ (M^{-1} s^{-1}) for the TIM-catalyzed reactions of the minor *free carbonyl* form of [1-^{13}C]-GA that were calculated from the values of k_{obsd} using eq 13, where f_{hyd} = 0.94 is the fraction of GA present in the hydrated form (*19*). These apparent second-order rate constants for the reaction catalyzed by the chicken muscle enzyme are ca. 2-fold smaller than those determined earlier for the enzyme from rabbit muscle under the same reaction conditions (*19*).

$$(k_{cat}/K_m)_{obsd} = \frac{k_{obsd}}{(1 - f_{hyd})[TIM]} \quad (13)$$

Unactivated TIM-Catalyzed Reaction of [1-^{13}C]-GA in the Absence of Phosphite. In the absence of phosphite dianion

Table 1: Product Distributions for the Reaction of [1-^{13}C]-Glycolaldehyde Catalyzed by Chicken Muscle Triosephosphate Isomerase in D_2O in the Absence and Presence of Phosphite Dianion[a]

			initial normalized product yield f_E[b]		
[TIM] (μM)	[HPO_3^{2-}] (mM)	$(k_{cat}/K_m)_{obsd}$[c] (M^{-1} s^{-1})	[2-^{13}C]-GA	[2-^{13}C,2-^{2}H]-GA	[1-^{13}C,2-^{2}H]-GA
340	none[d]	0.19	0.10 ± 0.01	0.60 ± 0.01	0.30 ± 0.01
7.9	5[e]	12.6	0.12 ± 0.003	0.65 ± 0.01	0.22 ± 0.01
5.5	10[e]	21.0	0.13 ± 0.003	0.64 ± 0.004	0.23 ± 0.01
2.5	20[e]	33.7	0.12 ± 0.003	0.64 ±0.003	0.23 ± 0.005
	average[f]		0.12	0.64	0.23
			$k_{ex}/(k_{C1})_H$ = 7.3[g]	$(k_{C2})_D/(k_{C1})_D$ = 0.36[h]	

[a] For reactions at pD 7.0, 25 °C, and I = 0.1 (NaCl). [b] The normalized product yields at various reaction times were determined by ^{1}H NMR spectroscopy, as described in the text. The initial normalized product yields f_E were determined as the y-intercept of the plots of f_P against time shown in Figure 2. The quoted errors are standard deviations in these intercepts. [c] Apparent second-order rate constant for the TIM-catalyzed reaction calculated from the observed first-order rate constant for the reaction using eq 13. [d] Buffered by 24 mM imidazole (20% free base). [e] Buffered by phosphite (50% free base) and 6 mM imidazole (20% free base). [f] Average of the values of f_E for the phosphite-activated TIM-catalyzed reactions. [g] Rate constant ratio for partitioning of the TIM·enediol(ate) complex labeled with hydrogen at Glu-165 between hydron exchange with solvent D_2O and intramolecular transfer of the substrate-derived hydrogen to form [2-^{13}C]-GA. [h] Rate constant ratio for partitioning of the TIM·enediol(ate) complex labeled with deuterium at Glu-165 between deuterium transfer to give [1-^{13}C,2-^{2}H]-GA (exchange) and [2-^{13}C,2-^{2}H]-GA (isomerization with exchange).

we observe only a very sluggish chicken muscle TIM-catalyzed reaction of [1-^{13}C]-GA in D_2O at pD 7.0 and 25 °C. The value of $(k_{cat}/K_m)_{obsd} = 0.19\ M^{-1}\ s^{-1}$ for this reaction (Table 1) is similar to $(k_{cat}/K_m)_{obsd} = 0.26\ M^{-1}\ s^{-1}$ that we reported for the deuterium exchange reaction of unlabeled GA catalyzed by rabbit muscle TIM under the same reaction conditions (*19*).

Panels C and D of Figure 1 show partial ^{1}H NMR spectra at 500 MHz in the region of the C-1 and C-2 protons, respectively, obtained after the reaction of 29% of [1-^{13}C]-GA (20 mM) catalyzed by chicken muscle TIM (340 μM) in D_2O at pD 7.0, 25 °C, and $I = 0.1$ (NaCl). The spectrum in the region of the C-2 protons (Figure 1D) shows that the unactivated TIM-catalyzed reaction results in formation of the same three isomerization and deuterium exchange products that are observed for the phosphite-activated reaction (Scheme 4). However, the total concentration of these products, calculated from the normalized peak areas of a single C-2 proton of each, is only ca. 50% of the calculated decrease in the concentration of the reactant [1-^{13}C]-GA. We reported previously that there are slow nonspecific protein-catalyzed reactions of unlabeled GA (*19*) and of (*R*)-glyceraldehyde (*10*) that occur *outside* the active site of TIM. By analogy, we conclude that the three products that are observed for the TIM-catalyzed reaction of [1-^{13}C]-GA in D_2O both in the presence and in the absence of phosphite dianion result from the *specific* reaction of GA bound in the active site of TIM. However, slow *nonspecific* reaction(s) that occur outside the active site compete with the specific reaction and result in formation of other products.

There is good evidence that a major product of the *nonspecific* TIM-catalyzed reaction of [1-^{13}C]-GA in D_2O is [1-^{13}C,2,2-$^2H_2$]-GA, resulting from deuterium exchange of both C-2 protons. After disappearance of 29% of [1-^{13}C]-GA in the *unactivated* TIM-catalyzed reaction the ratio of the areas of the three downfield peaks of the *apparent* double triplet due to the C-1 proton is 1.00:2.10:1.36 (Figure 1C, inset). By contrast, after disappearance of 23% of [1-^{13}C]-GA in the *phosphite-activated* TIM-catalyzed reaction this ratio is 1.00:2.18:1.17 (Figure 1A). The anomalous peak ratio observed for the unactivated TIM-catalyzed reaction can be attributed to a large shoulder on the downfield side of the most upfield peak of each half of the *apparent* double triplet (Figure 1C, inset). We assign this shoulder to the C-1 proton of [1-^{13}C,2,2-$^2H_2$]-GA which lacks a C-2 proton. The signal for [2,2-$^2H_2$]-GA formed during the rabbit muscle TIM-catalyzed reaction of GA in D_2O is broad singlet shifted 0.009 ppm upfield of the triplet due to GA, and it appears as a larger shoulder on the downfield side of the most upfield peak of this triplet (*19*). The presence of this shoulder is reflected in a higher yield of the deuterium-labeled product(s) of the unactivated TIM-catalyzed reactions of [1-^{13}C]-GA calculated using the peak area for the C-1 proton (eq 7) than that calculated using the peak area of the C-2 proton (eq 8). These ^{1}H NMR spectral data were used to calculate an absolute yield of 17% [1-^{13}C,2,2-$^2H_2$]-GA which brings the total absolute yield of the products of the unactivated TIM-catalyzed reaction in the absence of phosphite dianion ([2-^{13}C]-GA, [2-^{13}C,2-^{2}H]-GA, [1-^{13}C,2-^{2}H]-GA, and [1-^{13}C,2,2-$^2H_2$]-GA) to 70%. We have not characterized the other product(s) that are formed under these reaction conditions.

The fractional yields of the products of the *specific* reaction of [1-^{13}C]-GA in the active site of TIM, [2-^{13}C]-GA, [2-^{13}C,2-^{2}H]-GA, and [1-^{13}C,2-^{2}H]-GA, f_P, were calculated using the normalized peak areas for the better resolved C-2 protons of the reactants and products using eq 12, which normalizes the yields to a total of 100%. Table 1 gives the *initial normalized* product yields, f_E, that were obtained from short extrapolations of the observed yields to zero time.

DISCUSSION

We reported earlier that the reaction of unlabeled GA catalyzed by TIM in D_2O is only partially inhibited by a saturating concentration of the competitive inhibitor 2-phosphoglycolate (*19*). We concluded that there is a *nonspecific* protein-catalyzed reaction of GA that occurs outside the active site of TIM at a rate similar to that of the specific reaction of GA within the active site. This "external" reaction does not make a significant contribution to either the observed rate or the product distribution for the TIM-catalyzed reaction of [1-^{13}C]-GA in the presence of ≥5 mM phosphite dianion, because the phosphite-activated reaction is at least 60-fold faster than the unactivated reaction (Table 1) (*19*). The observation that the unactivated TIM-catalyzed isomerization of GA within the enzyme active site occurs at a similar rate to that of the competing reaction(s) of GA on the protein surface emphasizes the crippling effect of removal of the substrate phosphodianion group on enzyme activity. Comparison of the product distributions for the TIM-catalyzed reaction of [1-^{13}C]-GA in the presence and absence of phosphite dianion provides considerable insight into the reaction mechanism.

Phosphite-Activated TIM-Catalyzed Reaction of [1-^{13}C]-GA. Table 1 gives the yields of the products of the phosphite-activated TIM-catalyzed reaction of [1-^{13}C]-GA in D_2O in the presence of several concentrations of phosphite dianion, determined by ^{1}H NMR analysis (Figure 1). Figure 3 compares the product distribution for this reaction with those from our earlier work for the TIM-catalyzed reactions of the natural phosphorylated substrates GAP (*22*) and DHAP (*23*) in D_2O. These data provide strong evidence that the TIM-catalyzed reactions of the phosphodianion substrates and the phosphite-activated reaction of [1-^{13}C]-GA each occur within the confines of the active site of the loop-closed enzyme, where the substrate is sequestered from bulk solvent (*22*, *23*, *34*). However, there are differences between these product distributions that we cannot rationalize fully. One problem is that we are unable to rigorously define the pathways for the phosphite-activated reaction of [1-^{13}C]-GA because this substrate can bind in the active site in two different configurations relative to the cobound phosphite dianion, resembling the binding of the whole substrate GAP or DHAP (Scheme 5).[2] There is nothing known about the relative reactivity of [1-^{13}C]-GA bound in these different configurations, but reaction in either configuration can lead to formation of the same three reaction products shown in Scheme 4 and Figure 3.

The yield of the isomerization product [2-^{13}C]-GA from the TIM-catalyzed reaction of [1-^{13}C]-GA with intramolecular transfer of hydrogen (12%) is much smaller than the yield of the corresponding

[2]The data in Table 1 show that TIM catalyzes the isomerization of [1-^{13}C]-GA in the presence of phosphite dianion to give [2-^{13}C]-GA, a reaction that exchanges the positions of the carbonyl and hydroxymethylene carbons of the substrate relative to the enzyme-bound phosphite dianion piece (Scheme 5). The principle of microscopic reversibility then requires that TIM also catalyze the isomerization of [1-^{13}C]-GA cobound with phosphite dianion in either the reactant or the isomerized product configuration. We have also observed that TIM catalyzes the exchange of both the *pro-R* and the *pro-S* hydrogens of unlabeled GA for deuterium from solvent D_2O (unpublished results). This reflects the differing stereoselectivities for deprotonation of the bound GA piece by TIM when it is bound in the GAP (abstraction of the *pro-S* hydrogen) and DHAP (abstraction of the *pro-R* hydrogen) configurations (Scheme 5).

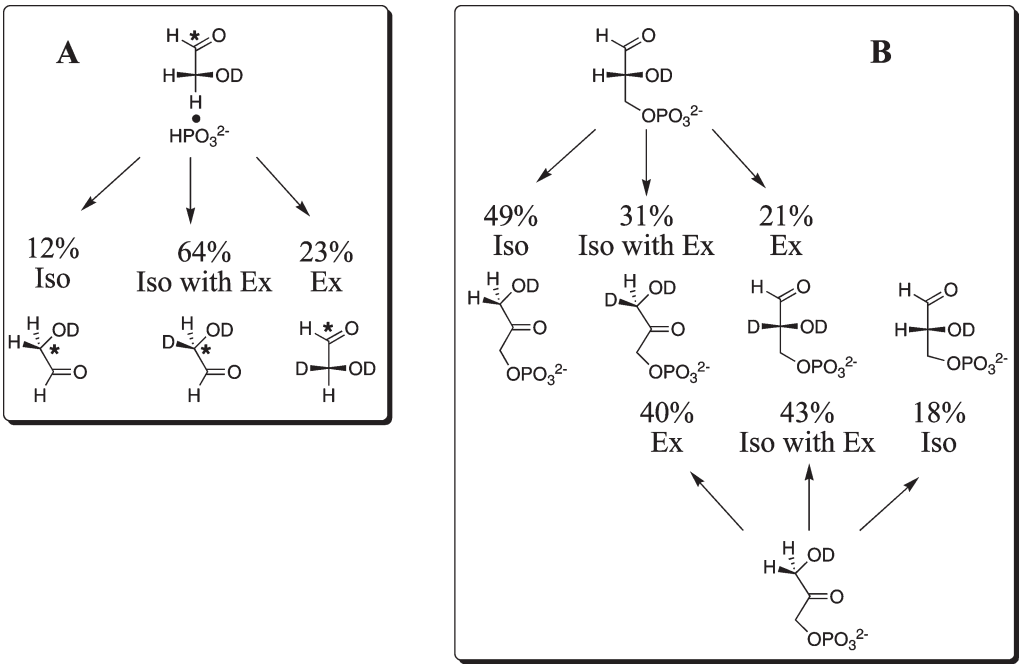

FIGURE 3: Product distributions for the turnover of carbon acid substrates by TIM in D_2O at 25 °C. (A) Product distribution for the reaction of [1-^{13}C]-GA catalyzed by chicken muscle TIM in the presence of 5 mM phosphite dianion at pD 7.0 (this work). (B) Product distributions for the reactions of GAP and DHAP catalyzed by rabbit or chicken muscle TIM at pD 7.9 from our earlier work (*22*, *23*).

Scheme 5

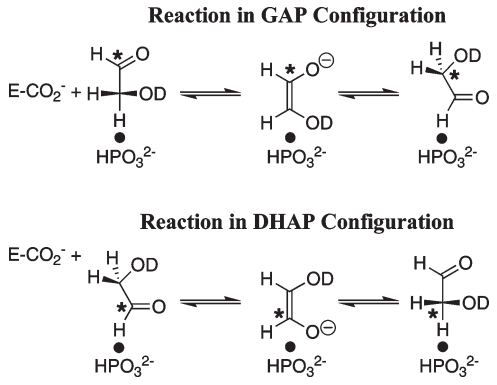

product of the TIM-catalyzed reaction of GAP (DHAP, 49%) but similar to the yield of the isomerization product of the TIM-catalyzed reaction of DHAP (GAP, 18%). We suggest (a) that [1-^{13}C]-GA reacts preferentially in the DHAP configuration (Scheme 5) and (b) that the greater conformational flexibility of the TIM-bound substrate pieces phosphite and [1-^{13}C]-GA, compared with TIM-bound triose phosphates, favors exchange of the H-labeled carboxylate side chain of Glu-165 with deuterium from solvent within the restricted confines of the active site at the loop-closed enzyme.

Figure 3 shows that the phosphite-activated TIM-catalyzed reaction of [1-^{13}C]-GA in D_2O gives a ca. 3-fold greater yield of the product of isomerization with deuterium incorporation ([2-^{13}C,2-^{2}H]-GA, 64%) than of the product representing deuterium incorporation into the remaining substrate ([1-^{13}C,2-^{2}H]-GA, 23%). A similar, but smaller, preference for incorporation of deuterium into the isomerization product, compared to incorporation into the remaining substrate, is observed for the reactions of both GAP (31% [1-^{2}H]-DHAP and 21% [2-^{2}H-GAP]) (*22*) and DHAP (43% [2-^{2}H]-GAP and 40% [1-^{2}H]-DHAP) (*23*). The H95Q mutation at TIM removes the imidazole side chain that stabilizes the negative charge at O-1 and/or O-2 of the enediol(ate) phosphate intermediate for the wild-type enzyme (*35*−*37*) and results in an even more striking difference in the partitioning of the intermediates of the reactions of DHAP and GAP. The reaction of DHAP catalyzed by H95Q mutant yeast TIM in $^{3}H_2O$ results in the incorporation of tritium label exclusively into the product GAP, while the reaction of GAP results in the incorporation of tritium label exclusively into the product DHAP (*37*). A "criss-cross" pathway for hydron exchange between O-1 and O-2 of the enediol(ate) phosphate intermediate was suggested to explain these results (*37*−*39*). If the imidazole side chain of His-95 at wild-type TIM provides a second competing pathway for hydron exchange between O-1 and O-2 (*23*, *34*) that allows for the exchange of deuterium from solvent into *unreacted* substrate shown in Figure 3, then the partial operation of this "criss-cross" pathway could explain the observed product distributions for the wild-type enzyme-catalyzed reactions of both whole substrates GAP and DHAP and of the substrate pieces {[1-^{13}C]-GA + HPO_3^{2-}} (Figure 3).

Unactivated TIM-Catalyzed Reaction of [1-^{13}C]-GA. We have not attempted to characterize all of the products of the slow *nonspecific* reaction of [1-^{13}C]-GA catalyzed by TIM in D_2O. Table 1 gives the yields of the unactivated TIM-catalyzed reaction of [1-^{13}C]-GA in D_2O in the absence of phosphite, determined by ^{1}H NMR analysis, that were normalized to a total of 100%. There is a somewhat higher yield of [1-^{13}C,2-^{2}H]-GA, and correspondingly lower yields of [2-^{13}C]-GA and [2-^{13}C,2-^{2}H]-GA, than for the activated reactions in the presence of phosphite dianion. These results are consistent with the formation of additional [1-^{13}C,2-^{2}H]-GA (ca. 10% of the total of the three products shown in Scheme 4) from slow competing *nonspecific* protein-catalyzed exchange of the C-2 proton of [1-^{13}C]-GA for deuterium from solvent. The ratio of the yields of the isomerization products [2-^{13}C]-GA and [2-^{13}C,2-^{2}H]-GA from the unactivated TIM-catalyzed reaction of [1-^{13}C]-GA (0.10/0.60) is the same, within experimental error, as that for the phosphite-activated reaction (0.12/0.64). The formation of additional [1-^{13}C,2-^{2}H]-GA in a nonspecific protein-catalyzed reaction by

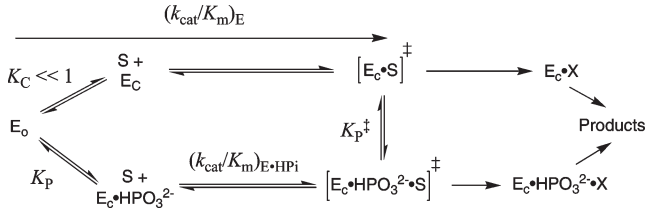

FIGURE 4: Proposed mechanisms for the unactivated and phosphite-activated deprotonation of glycolaldehyde by TIM to give an enzyme-bound enediol(ate) intermediate X. The direct unactivated reaction of glycolaldehyde, $(k_{cat}/K_m)_E$, is slow because free TIM exists mainly in the inactive loop-open form E_O that is in equilibrium with a high-energy active loop-closed form E_C ($K_C \ll 1$). Phosphite dianion binds selectively to E_C and stabilizes the active loop-closed enzyme relative to inactive E_O. The observed second-order rate constant for the reaction catalyzed by the $E_c \cdot HPO_3^{2-}$ complex, $(k_{cat}/K_m)_{E \cdot HPi}$, is much larger than $(k_{cat}/K_m)_E$ for the unactivated reaction (*19*).

an independent pathway should result in the same proportional decrease in the yields of [2-^{13}C]-GA and [2-^{13}C,2-^{2}H]-GA but no change in the ratio of these yields, as is observed.

We also observe the formation of the doubly deuterated product [1-^{13}C,2,2-$^{2}H_2$]-GA (17% yield, based on *total* products calculated from the disappearance of [1-^{13}C]-GA) which we propose is a major product of the *nonspecific* protein-catalyzed reaction of [1-^{13}C]-GA. We suggest that this nonspecific reaction involves the formation of a Schiff's base(s) between the alkylamino side chain(s) of lysine at TIM and [1-^{13}C]-GA to give a reactive iminium ion that undergoes rapid base-catalyzed deuterium exchange of the C-2 proton through an enamine intermediate (Scheme 6). We observe no lag in the formation of the doubly deuterated product [1-^{13}C,2,2-$^{2}H_2$]-GA, which suggests that exchange of a second deuterium at the Schiff's base adduct is significantly faster than its hydrolysis to regenerate the free enzyme and the singly labeled [1-^{13}C,2-^{2}H]-GA (Scheme 6). Model studies of the dedeuteration reaction of acetone-d_6 in H_2O show that diamines act as bifunctional catalysts of hydron exchange and that formation of the iminium ion adduct results in multiple intramolecular amine-catalyzed hydron exchange reactions that are much faster than hydrolysis of the iminium ion to regenerate the ketone and diamine (*40*, *41*).

Scheme 6

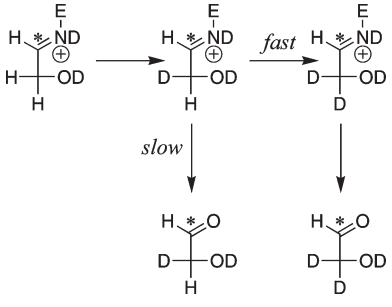

Mechanism of Activation of TIM by Phosphite Dianion. X-ray crystallographic data show that the binding interactions between the flexible "phosphate gripper" loop (loop 6) at TIM and the phosphodianion group of bound DHAP (*7*, *42*) or the intermediate analogues 2-phosphoglycolate (*43*) or phosphoglycolohydroxamate (*44*) draw loop 6 over the bound ligand to close the active site. Figure 4 shows this conversion of TIM from the major inactive loop-open form (E_o) to the rare active loop-closed form (E_c) ($K_C \ll 1$) (*19*). The observation of similar relative yields of the isomerization products [2-^{13}C]-GA and [2-^{13}C,2-^{2}H]-GA for the unactivated (0.10/0.60) and phosphite-activated (0.12/0.64) TIM-catalyzed reactions of [1-^{13}C]-GA in D_2O shows that the dianion activator affects the *rate*, but not the *product distribution*, of these two TIM-catalyzed reactions at the enzyme active site. Our data are consistent with the conclusion that both reactions involve partitioning of the enzyme-bound enediol(ate) intermediate (X, Figure 4) at the same loop-closed enzyme. We therefore suggest that the reaction of [1-^{13}C]-GA proceeds by the (conceptual) binding of the carbon acid substrate to this rare loop-closed enzyme form. In this model phosphite dianion activation then results from utilization of its intrinsic binding energy (*21*) specifically to stabilize the catalytically active closed enzyme form ($E_c \cdot HPO_3^{2-}$) and increase its concentration in water (Figure 4) (*19*).

REFERENCES

1. Knowles, J. R., and Albery, W. J. (1977) Perfection in enzyme catalysis: the energetics of triosephosphate isomerase. *Acc. Chem. Res. 10*, 105–111.
2. Rieder, S. V., and Rose, I. A. (1959) Mechanism of the triose phosphate isomerase reaction. *J. Biol. Chem. 234*, 1007–1010.
3. Shonk, C. E., and Boxer, G. E. (1964) Enzyme patterns in human tissues. I. Methods for the determination of glycolytic enzymes. *Cancer. Res. 24*, 709–721.
4. Gerlt, J. A., and Gassman, P. G. (1993) Understanding the rates of certain enzyme-catalyzed reactions: proton abstraction from carbon acids, acyl-transfer reactions, and displacement reactions of phosphodiesters. *Biochemistry 32*, 11943–11952.
5. Amyes, T. L., and Richard, J. P. (2007) Proton transfer to and from carbon in model systems, in *Hydrogen-Transfer Reactions*, *Vol. 3*, Biological Aspects I-II (Hynes, J. T., Klinman, J. P., Limbach, H.-H., and Schowen, R. L., Eds.) pp 949−973, Wiley-VCH, Weinheim.
6. Xiang, J., Jung, J.-y., and Sampson, N. S. (2004) Entropy effects on protein hinges: The reaction catalyzed by triosephosphate isomerase. *Biochemistry 43*, 11436–11445.
7. Jogl, G., Rozovsky, S., McDermott, A. E., and Tong, L. (2003) Optimal alignment for enzymatic proton transfer: Structure of the Michaelis complex of triosephosphate isomerase at 1.2 Å resolution. *Proc. Natl. Acad. Sci. U.S.A. 100*, 50–55.
8. Loria, J. P., Berlow, R. B., and Watt, E. D. (2008) Characterization of enzyme motions by solution NMR relaxation dispersion. *Acc. Chem. Res. 41*, 214–221.
9. Blacklow, S. C., Raines, R. T., Lim, W. A., Zamore, P. D., and Knowles, J. R. (1988) Triosephosphate isomerase catalysis is diffusion controlled. *Biochemistry 27*, 1158–1165.
10. Amyes, T. L., O'Donoghue, A. C., and Richard, J. P. (2001) Contribution of phosphate intrinsic binding energy to the enzymatic rate acceleration for triosephosphate isomerase. *J. Am. Chem. Soc. 123*, 11325–11326.
11. Richard, J. P. (1984) Acid-base catalysis of the elimination and isomerization reactions of triose phosphates. *J. Am. Chem. Soc. 106*, 4926–4936.
12. Pompliano, D. L., Peyman, A., and Knowles, J. R. (1990) Stabilization of a reaction intermediate as a catalytic device: definition of the functional role of the flexible loop in triosephosphate isomerase. *Biochemistry 29*, 3186–3194.
13. Sampson, N. S., and Knowles, J. R. (1992) Segmental movement: definition of the structural requirements for loop closure in catalysis by triosephosphate isomerase. *Biochemistry 31*, 8482–8487.
14. Sampson, N. S., and Knowles, J. R. (1992) Segmental motion in catalysis: investigation of a hydrogen bond critical for loop closure in the reaction of triosephosphate isomerase. *Biochemistry 31*, 8488–8494.
15. Sun, J., and Sampson, N. S. (1999) Understanding protein lids: kinetic analysis of active hinge mutants in triosephosphate isomerase. *Biochemistry 38*, 11474–11481.
16. Xiang, J., Sun, J., and Sampson, N. S. (2001) The importance of hinge sequence for loop function and catalytic activity in the reaction catalyzed by triosephosphate isomerase. *J. Mol. Biol. 307*, 1103–1112.
17. Kursula, I., Salin, M., Sun, J., Norledge, B. V., Haapalainen, A. M., Sampson, N. S., and Wierenga, R. K. (2004) Understanding protein lids: structural analysis of active hinge mutants in triosephosphate isomerase. *Protein Eng., Des. Sel. 17*, 375–382.
18. Sun, J., and Sampson, N. S. (1998) Determination of the amino acid requirements for a protein hinge in triosephosphate isomerase. *Protein Sci. 7*, 1495–1505.

19. Amyes, T. L., and Richard, J. P. (2007) Enzymatic catalysis of proton transfer at carbon: activation of triosephosphate isomerase by phosphite dianion. *Biochemistry 46*, 5841–5854.
20. Tsang, W.-Y., Amyes, T. L., and Richard, J. P. (2008) A substrate in pieces: allosteric activation of glycerol 3-phosphate dehydrogenase (NAD^+) by phosphite dianion. *Biochemistry 47*, 4575–4582.
21. Jencks, W. P. (1975) Binding energy, specificity and enzymic catalysis: the Circe effect. *Adv. Enzymol. Relat. Areas Mol. Biol. 43*, 219–410.
22. O'Donoghue, A. C., Amyes, T. L., and Richard, J. P. (2005) Hydron transfer catalyzed by triosephosphate isomerase. Products of isomerization of (*R*)-glyceraldehyde 3-phosphate in D_2O. *Biochemistry 44*, 2610–2621.
23. O'Donoghue, A. C., Amyes, T. L., and Richard, J. P. (2005) Hydron transfer catalyzed by triosephosphate isomerase. Products of isomerization of dihydroxyacetone phosphate in D_2O. *Biochemistry 44*, 2622–2631.
24. Albery, W. J., and Knowles, J. R. (1976) Free-energy profile for the reaction catalyzed by triosephosphate isomerase. *Biochemistry 15*, 5627–5631.
25. Hermes, J. D., Parekh, S. M., Blacklow, S. C., Koster, H., and Knowles, J. R. (1989) A reliable method for random mutagenesis: the generation of mutant libraries using spiked oligodeoxyribonucleotide primers. *Gene 84*, 143–151.
26. Straus, D., and Gilbert, W. (1985) Chicken triosephosphate isomerase complements an *Escherichia coli* deficiency. *Proc. Natl. Acad. Sci. U.S.A. 82*, 2014–2018.
27. Putman, S. J., Coulson, A. F. W., Farley, I. R. T., Riddleston, B., and Knowles, J. R. (1972) Specificity and kinetics of triose phosphate isomerase from chicken muscle. *Biochem. J. 129*, 301–310.
28. Glasoe, P. K., and Long, F. A. (1960) Use of glass electrodes to measure acidities in deuterium oxide. *J. Phys. Chem. 64*, 188–190.
29. Collins, G. C. S., and George, W. O. (1971) Nuclear magnetic resonance spectra of glycolaldehyde. *J. Chem. Soc. B,* 1352–1355.
30. Plaut, B., and Knowles, J. R. (1972) pH-dependence of the triose phosphate isomerase reaction. *Biochem. J. 129*, 311–320.
31. Amyes, T. L., and Richard, J. P. (1992) Generation and stability of a simple thiol ester enolate in aqueous solution. *J. Am. Chem. Soc. 114*, 10297–10302.
32. Amyes, T. L., and Richard, J. P. (1996) Determination of the pK_a of ethyl acetate: Brønsted correlation for deprotonation of a simple oxygen ester in aqueous solution. *J. Am. Chem. Soc. 118*, 3129–3141.
33. Richard, J. P., Williams, G., O'Donoghue, A. C., and Amyes, T. L. (2002) Formation and stability of enolates of acetamide and acetate anion: an eigen plot for proton transfer at α-carbonyl carbon. *J. Am. Chem. Soc. 124*, 2957–2968.
34. O'Donoghue, A. C., Amyes, T. L., and Richard, J. P. (2008) Slow proton transfer from the hydrogen-labelled carboxylic acid side chain (Glu-165) of triosephosphate isomerase to imidazole buffer in D_2O. *Org. Biomol. Chem. 6*, 391–396.
35. Komives, E. A., Chang, L. C., Lolis, E., Tilton, R. F., Petsko, G. A., and Knowles, J. R. (1991) Electrophilic catalysis in triosephosphate isomerase: the role of histidine-95. *Biochemistry 30*, 3011–3019.
36. Lodi, P. J., and Knowles, J. R. (1991) Neutral imidazole is the electrophile in the reaction catalyzed by triosephosphate isomerase: structural origins and catalytic implications. *Biochemistry 30*, 6948–6956.
37. Nickbarg, E. B., Davenport, R. C., Petsko, G. A., and Knowles, J. R. (1988) Triosephosphate isomerase: removal of a putatively electrophilic histidine residue results in a subtle change in catalytic mechanism. *Biochemistry 27*, 5948–5960.
38. Harris, T. K., Abeygunawardana, C., and Mildvan, A. S. (1997) NMR studies of the role of hydrogen bonding in the mechanism of triosephosphate isomerase. *Biochemistry 36*, 14661–14675.
39. Harris, T. K., Cole, R. N., Comer, F. I., and Mildvan, A. S. (1998) Proton transfer in the mechanism of triosephosphate isomerase. *Biochemistry 37*, 16828–16838.
40. Hine, J. (1978) Bifunctional catalysis of α-hydrogen exchange of aldehydes and ketones. *Acc. Chem. Res. 11*, 1–7.
41. Hine, J., and Li, W. (1976) Catalysis of α-hydrogen exchange. XIX. Bifunctional catalysis of the dedeuteration of acetone-d_6 by conformationally constrained derivatives of *N*,*N*-dimethyl-1,3-propanediamine. *J. Am. Chem. Soc. 98*, 3287–3294.
42. Alber, T., Banner, D. W., Bloomer, A. C., Petsko, G. A., Phillips, D., Rivers, P. S., and Wilson, I. A. (1981) On the three-dimensional structure and catalytic mechanism of triose phosphate isomerase. *Philos. Trans. R. Soc. London, Ser. B 293*, 159–171.
43. Lolis, E., and Petsko, G. A. (1990) Crystallographic analysis of the complex between triosephosphate isomerase and 2-phosphoglycolate at 2.5-Å resolution: implications for catalysis. *Biochemistry 29*, 6619–6625.
44. Davenport, R. C., Bash, P. A., Seaton, B. A., Karplus, M., Petsko, G. A., and Ringe, D. (1991) Structure of the triosephosphate isomerase-phosphoglycolohydroxamate complex: an analog of the intermediate on the reaction pathway. *Biochemistry 30*, 5821–5826.